EUROPEAN POLYMER JOURNAL

VOLUME 49, ISSUE 10, OCTOBER 2013, PAGES 3104–3113

http://dx.doi.org/10.1016/j.eurpolymj.2013.07.007

http://www.sciencedirect.com/science/article/pii/S0014305713003480

STRUCTURE, PROPERTIES AND INTERFACIAL INTERACTIONS IN POLY(LACTIC ACID)/POLYURETHANE BLENDS PREPARED BY REACTIVE PROCESSING

Balázs Imre[1,2,*], Dániel Bedő[1,2], Attila Domján[3], Peter Schön[4], G. Julius Vancsó[4] and Béla Pukánszky[1,2]

[1]Laboratory of Plastics and Rubber Technology, Budapest University of Technology and Economics, H-1521 Budapest, P.O. Box 91, Hungary

[2]Institute of Materials and Environmental Chemistry, Research Centre for Natural Sciences, Hungarian Academy of Sciences, H-1525 Budapest, P.O. Box 17, Hungary

[3]Institute of Organic Chemistry, Research Centre for Natural Sciences, Hungarian Academy of Sciences, H-1525 Budapest, P. O. Box 17, Hungary

[3]Materials Science and Technology of Polymers, MESA[+] Institute for Nanotechnology, University of Twente, Enschede, NL-7500, The Netherlands

*Corresponding author: Phone: +36-1-463-2967, Fax: +36-1-463-3474, Email: bimre@mail.bme.hu

ABSTRACT

Polyurethane elastomers are promising candidates for the impact modification of PLA producing blends for example for biomedicine. Poly(lactic acid) (PLA)/polyurethane elastomer (PU) blends were prepared by reactive processing and physical blending as comparison. The blends were characterized by a number of techniques including microscopy (scanning electron microscopy, SEM, and atomic force microscopy, AFM), rotational viscometry, thermal (dynamic mechanical analysis), DMA, and mechanical (tensile) measurements. The analysis and comparison of the structure and properties of physical and reactor blends proved the successful coupling of the phases. Coupling resulted in more advantageous structure and superior mechanical properties compared to those of physical blends as confirmed by morphology, macroscopic properties and the quantitative estimation of interfacial interactions. Structural studies and the composition dependence of properties indicated the formation of a submicron, phase-in-phase structure which positively influenced properties at large PU contents. The results strongly support that reactive processing is a convenient, cost-effective and environmentally friendly technique to obtain blends with superior properties.

KEYWORDS: reactive blending, compatibilization, PLA, polyurethane elastomer, phase structure, interfacial interactions

1. INTRODUCTION

The interest in using polymeric materials derived from renewable resources increases by the day because of the considerably improved environmental awareness of society and concerns about the depletion of petrochemical based plastics [1]. Poly(lactic acid), PLA, seems to be a polymer of choice which satisfies this surge of demand, the requirements of large scale processing and application, at the same time. PLA has several advantages, among others it can be produced from renewable resources [2] thus its application does not generate supplementary CO_2 emission [3], it is recyclable and compostable, it has good stiffness and strength, and its properties can be modified and adjusted to a large number of applications in various ways [4-6]. On the other hand, this polymer has some drawbacks as well, including moisture sensitivity, fast physical ageing, poor impact resistance and relatively high price [4-6]. As a consequence, many attempts have been made to modify it by plasticization [7-13], copolymerization [14-19], blending [20,21] or by the production of particulate filled or fiber reinforced composites [11-13,22-30].

Physical ageing leading to increased stiffness and de-

creased deformability contribute significantly to the poor fracture resistance of PLA. Many attempts have been made to improve impact resistance by blending it with elastomers. Poly(ε-caprolactone) PCL, for example, is a biodegradable polymer with excellent deformability and impact properties, thus it appears to be very appropriate for the modification of PLA. Unfortunately, the melt blending of the two polymers results in marginal improvement of toughness at the price of a considerable decrease in stiffness and strength as a result of complete immiscibility and weak interfacial adhesion [31, 32]. In order to improve compatibility and achieve a more advantageous combination of properties, several methods have been applied, e.g. the addition of block copolymers such as PCL-PLA diblock [33-35], triblock [33, 36, 37] and random copolymers, a PCL-PEG copolymer [38], a PEO-PPO-PEO triblock copolymer [39] or several commercial impact modifiers [40] with various successes.

Biopolymers often contain a number of reactive groups offering excellent possibility for the reactive compatibilization of their blends. The addition of a compound miscible with one blend component and reactive towards the functional groups of the other results in the in situ formation of grafted or block-copolymers acting as compatibilizers [41-43]. The method possesses considerable potential, since structure and properties can be controlled

relatively easily by the proper selection of components, blend composition and processing conditions. Two or multiple step compatibilization by maleic anhydride is a good example for this approach [44-46]. However, one-step blending and compatibilization possesses several advantages, both from an economical and environmental point of view, since it enables the elimination of several processing steps. Such a process was reported by Dubois et al. [47, 48] more than ten years ago. The ring-opening polymerization (ROP) of cyclic esters initiated by the hydroxyl groups of biopolymers like starch [47], dextran [48] or partially substituted cellulose acetate [49-51] is a convenient method for the preparation of block copolymers via reactive processing, although various other combinations are also possible.

The goal of this study was to prepare PLA-PU blends with improved properties compared to those of PLA. Blends were prepared by reactive processing and physical blending. The coupling of the components was achieved in the reactive blends through the isocyanate group reacting with the hydroxyl and carboxyl end-groups of PLA, which results in the formation of PLA-b-PU block copolymer acting as compatibilizer. Reactive blends (PLA-b-PU) are compared to samples with the same composition but prepared by physical blending (PLA/PU).

2. EXPERIMENTAL

The PLA used in the experiments was obtained from NatureWorks (USA). The selected grade (Ingeo 4032D, M_n = 88500 g/mol and M_w/M_n = 1.8) is recommended for extrusion. The polymer (<2 % D isomer) has a density of 1.24 g/cm^3, while its melt flow index (MFI) is 3.9 g/10 min at 190 °C and 2.16 kg load. Poly(tetrahydrofuran) (PTHF, M_n = 1000 g/mol), 1,4-butanediol (BD) and ′4,4 -methylenebis(phenyl isocyanate) (MDI) were obtained from Sigma-Aldrich for polyurethane synthesis. Both PLA and PTHF were dried in a vacuum oven before further use (110°C for 4 hours and 80 °C for 4 hours, respectively). Butanediol was vacuum-distilled in order to remove any traces of water, while MDI was used as received.

In the case of the two step polymerization and blending, polyurethane synthesis (150 °C, 50 rpm, 30 min) and the homogenization of PLA and PU (180 °C, 50 rpm, 12 min) were carried out in an internal mixer (Brabender W 50 EHT). The same equipment was used for the one-step method, i.e. reactive processing (180 °C, 50 rpm, 20 min). PLA was fed into the chamber first, followed by the addition of the diols (PTHF and BD) to the PLA melt and the isocyanate (MDI) was added last. Temperature and torque were recorded during homogenization. The melt was transferred to a Fontijne SRA 100 compression molding machine (190 °C, 5 min) to produce 1 mm

thick plates used for further testing.

Molecular weight was determined with size-exclusion chromatography (SEC). Chromatograms were recorded in dimethylformamide at a flow rate of 0.5 ml/min at 35 °C with a Waters chromatograph (Waters e2695 Separation Module) equipped with four gel columns (4.6 x 300 mm, 5 µm Styragel columns: HR 0.5, 1, 2 and 4) and a Waters 2414 refractive index detector. SEC was calibrated with polystyrene standards. The results were evaluated by the Empower 2 (Waters 2008) software.

The chemical structure of the reactor blends was characterized by selective dissolution and analysis. PLA was selectively extracted from the blends by dichloromethane. 2 g sample was extracted in 160 ml solvent for 48 hours. The extracted samples were dried in vacuum for 24 hours. The chemical structure and composition of the separated fractions were determined by solution state nuclear magnetic resonance spectroscopy (NMR). NMR spectra were obtained by a Varian Unity INOVA spectrometer operating at the ^{1}H frequency of 600 MHz with 5 mm inverse detection probe, while a Varian Unity INOVA spectrometer operating at the ^{1}H frequency of 400 MHz with a Z-gradient 5 mm inverse detection probe was used for ^{1}H diffusion-ordered spectroscopy (DOSY). The ^{1}H-DOSY experiments were carried out using a Performa I gradient amplifier with a 20 Gauss/cm maximum gradient capability. The bipolar

pulse-pair stimulated-echo (Dbppste) pulse sequence was used for acquiring diffusion data with 20 msec diffusion delay, 25 squared increments for gradient levels and 32 transients with a delay time of 16 sec. The Varian DOSY package was used for the processing. PLA and PU rich phases were dissolved in deuterated chloroform and dimethyl sulfoxide, respectively. The signals of the solvent were used as reference for chemical shifts. For the one-dimensional ^{1}H spectra 16 sec delay time and 4 sec acquisition time were used to get accurate integrals. Two-dimensional $^{1}H–^{13}C$ correlation spectra were recorded for assignation and to map the connections in a molecule. Homonuclear single-quantum correlation (HSQC) and heteronuclear multiple-quantum correlation (HMQC) measurements were carried out under standard conditions with 2 sec delay time to identify directly bonded C–H pairs and longer connections (2-3 bonds), respectively. The temperature of the measurements was 25 °C.

The glass transition temperature of the blends was determined via dynamic mechanical analysis (DMA) using a Perkin Elmer Diamond DMA apparatus. Measurements were done in tensile mode with constant amplitude (10 μm) and frequency (1 Hz) in a wide temperature range (-150-200 °C), with a heating rate of 2 °C/min. Rheological measurements were carried out using an Anton-Paar Physica MCR 301 apparatus at 180 °C in oscillatory mode in the frequency range of 0.1–600

1/sec on discs with 25 mm diameter and 1 mm thickness. The amplitude of the deformation was 2 %. The morphologies of the blends were studied by scanning electron microscopy (SEM, JEOL JSM-6380 LA) and AFM.

Atomic force micrographs were recorded on smooth, cryomicrotomed cross-sections of selected samples. A Multi-mode 8 AFM instrument equipped with a NanoScope V controller and NanoScope version 8.10 software (Bruker Nano Surface, Santa Barbara, CA, USA) was used for the AFM measurements. Image processing and data analysis were performed with the NanoScope software version 8.10, and NanoScope Analysis software version 1.40. Tapping mode imaging and Peak Force Tapping was done with Si cantilevers (RTESPA, Bruker AFM probes, Camarillo, CA, USA) in air. Cantilever spring constants were determined using the thermal tune method and showed values in the range of ~20-40 N/m. For DMT modulus measurements the cantilevers were calibrated using a standard PS sample. PeakForce Quantitative Nanomechanical Property Mapping (PF-QNM) AFM was done at a constant oscillation of the sample at 2 kHz using amplitudes of 150 nm. Scanning was performed at a speed of 1-2 lines/s.

Mechanical properties were characterized by tensile testing on standard ISO 527 5A specimens with a thickness of 1 mm, using an Instron 5566 apparatus. Stiffness (E) was determined at 0.5 mm/min cross-head speed and 50 mm gauge

length. Tensile strength (σ) and elongation-at-break (ε) were calculated from force vs. deformation traces measured on the same specimens at 5 mm/min cross-head speed.

3. RESULTS AND DISCUSSION

The results are presented and discussed in several sections. First the basic concept of forming block copolymers during reactive processing is presented, then the structure and properties of the obtained blends are discussed in subsequent sections. The important influence of interfacial interactions on properties is emphasized next and theoretical and practical consequences are considered in the final section.

3.1. Reactive processing

As mentioned earlier we anticipated that block copolymers can be formed from the two polymers through the reaction of the components of PU in the melt of PLA. The isocyanate group can react both with the hydroxyl and the acid end-groups of PLA, respectively. The possible reaction scenarios are presented in **Fig. 1**. Linear polymers form in the first two reactions, while a branched molecule results from the third. We also assumed that the polyol and the chain extender added would react with the chain end free isocyanate groups to create the block copolymer. The ratio

of the reacting functional groups, i.e. NCO/H(a), where H(a) indicates the number of groups containing active hydrogen on PTHF, BD and PLA end groups, was optimized in preliminary experiments to achieve maximum efficiency. This latter was estimated by changes in the mechanical properties of a PLA blend containing 30 vol% PU. The molar mass of the forming polyurethane shows strong correlation with the NCO/H(a) ratio affecting mechanical properties to a great extent. Tensile strength and elongation-at-break reached a constant value above the NCO/H(a) ratio of 1.01.

Using this stoichiometry, reactive (PLA-b-PU) blends were produced in the entire composition range from 0 to 1 PU content in 0.1 volume fraction steps. An example of reactive processing is presented in **Fig. 2** for the 50 vol% blend of PLA and PU. Torque proportional to viscosity was measured during homogenization and it is plotted against time in the figure, in which reactive processing is compared to traditional blending. In the latter case, torque decreases as temperature increases (not shown) to reach an equilibrium value at the end of homogenization. In reactive blending torque reaches a very small value after filling the mixer; reaction starts slowly then accelerates to produce the final polymer at the end of the process. Increasing torque is a positive sign showing that reactions take place during mixing and the result is a polymer with reasonable molar mass

and considerable viscosity. GPC measurements have shown that the molar mass of PU is similar to that of PLA, i.e. approximately 60000 g/mol. The formation of polyurethane as well as the coupling of the phases was confirmed by solution state NMR spectroscopy. PLA was selectively dissolved from the reactive blend containing 40 vol% PU, and the chemical structure of both phases was determined. The PU fraction contains only a small amount (less than 1 %) of impurities besides the polymer. In the PLA fraction, on the other hand, 3.7 PTHF, 3.0 BD and 6.7 MDI units were found to be attached to one PLA molecule in average, indicating the formation of PLA-b-PU block copolymers according to the reaction scheme presented in Fig. 1a. Signals belonging to acylurea and amide groups arising from the reaction of isocyanate with carboxyl were not detected, thus PU blocks form only on the hydroxyl PLA end-groups. However, We must point it out here, that although structural analysis unambiguously proved the formation of the PLA-b-PU block copolymer, its content is relatively small, and not all PLA chains reacted during processing.

3.2. Structure

The morphology of the blends was analyzed by SEM and AFM. Both methods showed heterogeneous structure in the physical and also in the reactor blends. Height and phase

imaging tapping mode AFM across the length scales were shown to be adequate techniques to investigate the microphase separated structures of polyurethanes [52-54]. Recently AFM based mechanical mapping techniques were able to determine the elastic moduli of phase separated PUs at nanoscale resolution [55]. To obtain sufficiently flat surfaces the PLA-PU samples were cryomicrotomed before AFM measurements. In tapping mode AFM phase imaging, the phase signal is related to the energy dissipation of the tapping tip originating from the adhesive and elastic properties of the inspected material surface. The color code in **Fig. 3** corresponds to variations in the phase signal, clearly showing two distinct domains indicative for the two blend components. Soft PU domains are represented by dark contrast, while the hard PLA domains appeared as bright areas [54]. The oriented structure of the blend most likely results from processing. The surface fractions measured by tapping mode AFM are in good agreement with the volume fractions used for the respective PLA-PU blend preparation.

Tapping mode AFM does not allow one to obtain quantitative mechanical maps because distinguishing adhesive and elastic contributions to the phase signal is impossible [56]. In order to be able to assign a specific domain with certainty to the tapping mode phase signal, complementing AFM based mechanical mapping was done (**Fig. 4**) providing

quantitative surface elastic moduli [57]. In a Peak Force Tapping experiment the local elastic modulus is estimated from the force distance curves using the Derjaguin–Müller–Toporov (DMT) mechanical contact model. According to the DMT model the forces of the AFM tip-surface interaction are

$$F_i = \frac{4}{3} E^* \sqrt{r(d - d_0)^3} + F_a \qquad (1)$$

where F_i is tip-sample-force, E^* reduced elastic modulus, r the contact radius of the AFM tip, d_0 surface rest position, $(d\text{-}d_0)$ the deformation of the sample and F_a is adhesion force. The DMT model was found to be useful for samples with moderate adhesion levels and AFM tips with small radii. Importantly, the approach and Eq. 1 allow feasible computation rendering it favorable for real time imaging.

Brighter domains revealed elastic modulus values around ~1 GPa assigned to the PLA phase, while the darker surrounding areas showed values <100 MPa indicative for the PU phase. As the AFM probe was calibrated for the harder PLA domain, a larger error is anticipated for the lower modulus value domains, although the elastic moduli observed are well in the regime of the respective bulk moduli for both polymers. Using the same AFM probe, a tapping mode phase image was recorded subsequently on the same sample area, revealing bright contrast for the PLA phase, consequently dark contrast for the PU domain.

A series of SEM micrographs is presented in **Fig. 5**,

which allows the comparison of the structure of the two kinds of blends. The effect of reactive processing can be clearly seen in the figure. The heterogeneity of the blends is obvious in all cases, but significant differences can also be observed. At small PU contents obviously PLA is the continuous phase, while this latter must be dispersed in PU at the other end of the composition range. It is difficult to identify the continuous phase at 50 vol% of both components, but AFM micrographs clearly prove that PU particles are dispersed in PLA even at this composition. Phase inversion seems to take place at around or somewhat above 50 vol% PU content. The apparent absence of an interpenetrating network type structure might indicate narrow phase inversion and poor interfacial interactions.

The comparison of physical blends to those produced by reactive processing indicates considerable changes in the size of the dispersed particles; particle size is always smaller in the reactor blend indicating the compatibilizing effect of block copolymer molecules. Particle size was determined quantitatively by taking a large number of micrographs from the blends. The result is presented in **Fig. 6**. Although the standard deviation of the data is quite large the tendency is clear. Particle size has a maximum as a function of composition in the composition range of phase transition, as expected, and the size of the dispersed par-

ticles is considerably smaller at all compositions in the reactor blend than in the material produced by simple mixing. The small particle size is a clear indication of improved interfacial interactions and the visual observation of SEM micrographs also confirms this conclusion, although micrographs taken from cryo-fractured surfaces cannot supply strong evidence on interfacial adhesion. Nevertheless, structure seems to indicate that reactive processing and coupling was successful as shown by chemical analysis.

Another aspect of structure, which contradicts the conclusion tentatively drawn from the study of SEM micrographs, is offered by the AFM micrograph presented in **Fig. 3**. The image was recorded on the PLA-b-PU reactor blend containing 50 vol% of both components. The possibility of a co-continuous phase structure is indicated by the figure, but more importantly the PU phase contains small PLA inclusions. The formation of such inclusions might result from the presence of PLA-b-PU block copolymer molecules, while their existence forecasts good interaction, but also to the possibility of the development of a structural formation of submicron scale at large PU contents. The formation of such a structure might influence properties considerably.

3.3. Properties

The composition dependence of some properties may give

information about changes in structure and interactions. However, not all properties respond to these factors equally sensitively and similarly. Properties measured at large deformations show the modification of interfacial adhesion much better than modulus, for example. The complex viscosity of selected physical blends is presented in **Fig. 7**. Reactor blends offer a very similar picture so the correlations are not shown here. Viscosity increases with increasing PU content in both cases, but to different extents. It is worth to note that viscosity does not approach a plateau value at low angular frequencies, but increases and the increase becomes stronger with increasing amounts of PU in the blend. The composition dependence of complex viscosity determined at 1 s^{-1} frequency is presented in **Fig. 8**. The difference between the two types of blends is striking, which indicates that reactive processing was effective indeed. While points lay below the straight line indicating additivity in the case of the physical blends indicating poor interaction of the phases, they are located above the line for the blend produced by reactive processing hinting to larger molecular weight and/or better adhesion. The large differences observed in the range of 60-90 vol% PU content are especially interesting, they indicate strong interaction and the formation of some internal or secondary structure, as mentioned already in the previous section (see **Fig. 3**).

We refrain from the presentation of all mechanical properties here. Because of the large discrepancy in the stiffness of the two components (3.2 GPa vs. ~10 MPa for PLA and PU, respectively) any differences caused by changes in structure or interfacial adhesion are very difficult to identify from the composition dependence of stiffness. Modulus is not very sensitive to changes of these factors anyway [58]. Yield and yield strain could be determined only when PLA was the continuous phase, i.e. below 50 vol% PU content. Deformability (elongation-at-break) showed some effect of blending technology, but large differences in inherent properties mask the effect of adhesion here too. On the other hand, tensile strength differs considerably for the two kinds of polymers. This property is plotted against PU content in **Fig. 9** together with representative AFM phase images to show the corresponding fine structure of the blends. Similar differences can be seen here as in **Fig. 8** in the composition dependence of complex viscosity. Properties are very similar at small PU content and differ considerably at the upper end of the composition range with a maximum at 90 vol% PU. The finer distribution of the dispersed phase and some kind of phase-in-phase structure is shown by the AFM micrographs recorded on the reactive blends (see also Fig. 3). The composition dependence of the properties and the corresponding microstructures prove that reactive processing was

effective and both the structure and the interfacial adhesion of the components improved as a result.

3.4. Interfacial interactions

SEM and AFM studies confirmed that structure is heterogeneous in both types of blends, i.e. the components are not miscible. Structure and properties are determined by the interaction of the components and both can vary in a very wide range in immiscible blends. For example, PVC forms large, 10 μm size particles in PP and the properties of their blends are extremely poor, while PP/PE blends possess much finer structure and better properties [59]. The quantitative estimation of interaction in blends is difficult. One can use the Flory-Huggins interaction parameter [60], but its determination and especially interpretation in reactor blends is questionable. Another approach is the determination and analysis of dynamic mechanical (DMA) spectra and the composition dependence of glass transition temperatures. Miscible blends usually exhibit a single glass transition temperature [61], while in immiscible blends transition temperatures shift toward each other to an extent depending on the mutual miscibility of the phases [62]. The DMA spectra of the PLA-b-PU blend containing 60 vol% PU is presented in **Fig. 10** as an example. The glass transition of the two components, i.e. PLA and PU can be clearly identified in the spectrum at

around 60 and -40 °C, respectively. Besides the two main transitions, a smaller one related to the soft segments of PU can be detected at around -80 °C, and the cold crystallization of PLA can be also observed at about 100 °C.

The glass transition temperatures of the two components are plotted against composition in **Fig. 11**. Quite surprisingly, they do not shift towards each other, on the contrary, the T_g of PLA increases, while that of PU decreases with increasing amount of the other component. The latter effect could be explained with the development of negative hydrostatic pressure as was observed in other blends of a stiff polymer with an elastomer [63**-65**], but the increase of the T_g of PLA needs further study. Such a change was observed also in PLA/thermoplastic starch blends and it must be related to changing interactions and/or the mobility of the PLA segments. Nevertheless, the higher T_g of the PU phase for the reactor blend indicates stronger interactions than those developing in the physical blend.

The strength of interfacial adhesion can be deduced also from the composition dependence of mechanical properties with the help of an approach developed earlier for particulate filled polymers and blends [59]. Accordingly, the composition dependence of any heterogeneous polymer system can be expressed as

$$\sigma_T = \sigma_{T0}\,\lambda^n \frac{1-\varphi}{1+2.5\varphi}\exp(B\varphi) \qquad (2)$$

where σ_T and σ_{T0} are the true tensile strength ($\sigma_T = \sigma\lambda$ and $\lambda = L/L_0$) of the composite and the matrix, respectively, n is a parameter expressing the strain hardening tendency of the matrix, φ is the volume fraction of the second component and B is related to the relative load-bearing capacity of this component, which depends on interfacial interaction. Taking into account the inherent properties of the components a parameter can be determined (C) which is related to interfacial interactions

$$B = \ln\frac{C\,\sigma_d}{\sigma_0} \qquad (3)$$

where σ_d is the strength of the dispersed component. According to **Eq. 2** by plotting the natural logarithm of reduced tensile strength [$\sigma_{Tred}=\sigma_T(1+2.5\varphi)/\sigma_{T0}\lambda^n(1-\varphi)$] against composition should yield a straight line the slope of which provides the value of parameter B and from that we can estimate the value of C. C was shown to correlate closely with the Flory-Huggins interaction parameter for a considerable number of blends [59].

The tensile strength of the blends was plotted in the linearized form as indicated above (see **Eq. 2**) in **Fig. 12**. We obtain straight lines in both cases with dissimilar slopes. The deviation from the straight line at large PU

content may be ascribed to phase inversion, while the deviation of the intersection from the matrix value may be caused by different structure or failure mechanism in the neat polymer and the matrix, respectively. We determined the value of parameter *B* from the slope of the lines and calculated *C*. We obtained 21.6 and 73.1 for the physical and the reactor blend, respectively. As comparison, a very small value of *C* = 2.9 was obtained for the PVC/PP blend of poor compatibility, while 39.9 for the miscible PPO/PS blend both prepared by physical mixing [59]. These values and the comparison show that interactions are reasonably strong already in the physical blend, but they are further improved by reactive blending.

4. CONCLUSIONS

The analysis and comparison of the structure and properties of physical blends and materials produced by reactive processing proved that the coupling of the phases was successful in the latter. Coupling resulted in more advantageous structure and properties than in physical blends as confirmed by morphology, macroscopic properties and the quantitative estimation of interfacial interactions. Structural studies and the composition dependence of properties indicated the development of a submicron structural formation which positively influenced properties at large PU

contents. The results provide strong evidence that reactive processing is a convenient, cost-effective and environmentally friendly technique to obtain blends with superior properties.

5. ACKNOWLEDGEMENTS

Virág Tuboly is acknowledged for her help in the preparation of the blends and Kristóf Bagdi for information and advice on PU elastomers. We are grateful for the assistance of József Hári and Károly Renner in the preparation of the SEM micrographs and for the help of György Deák with the GPC measurements. Clemens Padberg is gratefully acknowledged for supporting the AFM measurements. The financial support of the National Scientific Research Fund of Hungary (OTKA Grant No. K 101124) for the research on heterogeneous polymer systems is appreciated very much.

6. REFERENCES

1. Markarian J. Outdoor living space drives growth in wood-plastic composites. Plastics, Additives and Compounding 2008;10(4):20-25.
2. Sawyer DJ. Bioprocessing – no longer a field of dreams. Macromol Symp 2003;201(1):271-282.
3. Dorgan JR, Lehermeier HJ, Palade LI, Cicero J. Polylactides: properties and prospects of an environmen-

tally benign plastic from renewable resources. Macromol Symp 2001;175(1):55-66.

4. Auras R, Harte B, Selke S. An overview of polylactides as packaging materials. Macromol Biosci 2004;4(9):835-864.
5. Kale G, Auras R, Singh SP, Narayan R. Biodegradability of polylactide bottles in real and simulated composting conditions. Polym Test 2007;26(8):1049-1061.
6. Perego G, Cella GD. 11. Mechanical Properties. In Auras R, Lim L-T, Selke S, Tsuji H, editors. Poly(lactic acid): Synthesis, Structures, Properties, Processing, and Applications. New Jersey: John Wiley & Sons; 2010. p. 141-153.
7. Lemmouchi Y, Murariu M, Dos Santos AM, Amass AJ, Schacht E, Dubois P. Plasticization of poly(lactide) with blends of tributyl citrate and low molecular weight poly(D,L-lactide)-b-poly(ethylene glycol) copolymers. Eur Polym J 2009;45(10):2839-2848.
8. Pillin I, Montrelay N, Grohens Y. Thermo-mechanical characterization of plasticized PLA: is the miscibility the only significant factor? Polymer 2006;47(13):4676-4682.
9. Martin O, Avérous L. Poly(lactic acid): plasticization and properties of biodegradable multiphase systems. Polymer 2001;42(14):6209-6219.

10. Ljungberg N, Wesslen B. Tributyl citrate oligomers as plasticizers for poly (lactic acid): thermo-mechanical film properties and aging. Polymer 2003;44(25):7679-7688.
11. Wang N, Zhang XX, Ma XF, Fang JM. Influence of carbon black on the properties of plasticized poly(lactic acid) composites. Polym Degrad Stabil 2008;93(6):1044-1052.
12. Paul MA, Alexandre M, Degee P, Henrist C, Rulmont A, Dubois P. New nanocomposite materials based on plasticized poly(L-lactide) and organo-modified montmorillonites: thermal and morphological study. Polymer 2003;44(2):443-450.
13. Murariu M, Ferreira AD, Pluta M, Bonnaud L, Alexandre M, Dubois P. Polylactide (PLA)–CaSO4 composites toughened with low molecular weight and polymeric ester-like plasticizers and related performances. Eur Polym J 2008;44(11):3842-3852.
14. Li B, Chen SC, Qiu ZC, Yang QKK, Tang SP, Yu WJ, Wang YZ. Synthesis of poly(lactic acid-b-p-dioxanone) block copolymers from ring opening polymerization of p-dioxanone by poly(L-lactic acid) macroinitiators. Polym Bull 2008;61(2):139-146.
15. Hirata M, Kimura Y. Thermomechanical properties of stereoblock poly(lactic acid)s with different PLLA/PDLA block compositions. Polymer 2008;49(11):2656-2661.

16. Ho CH, Wang CH, Lin CI, Lee YD. Synthesis and characterization of TPO–PLA copolymer and its behavior as compatibilizer for PLA/TPO blends. Polymer 2008;49(18):3902-3910.
17. Mert O, Doganci E, Erbil HY, Dernir AS. Surface Characterization of Poly(l-lactic acid)–Methoxy Poly(ethylene glycol) Diblock Copolymers by Static and Dynamic Contact Angle Measurements, FTIR, and ATR-FTIR. Langmuir 2008;24(3):749-757.
18. Södergard A, Stolt M. Properties of Lactic Acid Based Polymers and Their Correlation With Composition. Prog Polym Sci 2002;27(6):1123-1163.
19. Nagahama K, Nishimura Y, Ohya Y, Ouchi T. Impacts of stereoregularity and stereocomplex formation on physicochemical, protein adsorption and cell adhesion behaviors of star-shaped 8-arms poly(ethylene glycol)–poly(lactide) block copolymer films. Polymer 2007;48(9):2649-2658.
20. Gu SY, Zhang K, Ren J, Zhan H. Melt rheology of polylactide/poly(butylene adipate-co-terephthalate) blends. Carbohydr Polym 2008;74(1):79-85.
21. Rohman G, Laupretre F, Boileau S, Guerin P, Grande D. Poly(d,l-lactide)/poly(methyl methacrylate) interpenetrating polymer networks: Synthesis, characterization,

and use as precursors to porous polymeric materials. Polymer 2007;48(24):7017-7028.

22. Pluta M, Jeszka JK, Boiteux G. Polylactide/montmorillonite nanocomposites: Structure, dielectric, viscoelastic and thermal properties. Eur Polym J 2007;43(7):2819-2835.
23. Gorna K, Hund M, Vucak M, Grohn F, Wegner G. Amorphous calcium carbonate in form of spherical nanosized particles and its application as fillers for polymers. Mater Sci Eng A: 2008;477(1-2):217-225.
24. Bleach NC, Nazhat SN, Tanner KE, Kellomaki M, Törmala P. Effect of filler content on mechanical and dynamic mechanical properties of particulate biphasic calcium phosphate--polylactide composites. Biomaterials 2002;23(7):1579-1585.
25. Bax B, Müssig J. Impact and tensile properties of PLA/Cordenka and PLA/flax composites. Compos Sci Technol 2008;68(7-8):1601-1607.
26. Kuan CF, Kuan HC, Ma CCM, Chen CH. Mechanical and electrical properties of multi-wall carbon nanotube/poly(lactic acid) composites. J Phys Chem Solids 2008;69(5-6):1395-1398.
27. Murariu M, Ferreira AD, Degee P, Alexandre M, Dubois P. Polylactide compositions. Part 1: Effect of filler con-

tent and size on mechanical properties of PLA/calcium sulfate composites. Polymer 2007;48(9):2613-2618.

28. Pluta M, Murariu M, Ferreira AD, Alexandre M, Galeski A, Dubois P. Polylactide compositions. II. Correlation between morphology and main properties of PLA/calcium sulfate composites (pages 2770–2780). J Polym Sci B Polym Phys 2007;45(19):2770-2780.
29. Sobkowicz MJ, Feaver JL, Dorgan JR. Clean and green bioplastic composites: Comparison of calcium sulfate and carbon nanospheres in polylactide composites. CLEAN-Soil Air Water 2008;36(8):706-713.
30. Kasuga T, Ota Y, Nogami M, Abe Y. Preparation and mechanical properties of polylactic acid composites containing hydroxyapatite fibers. Biomaterials 2001;22(1):19-23.
31. López-Rodríguez N, López-Arraiza A, Meaurio E, Sarasua JR. Crystallization, Morphology, and Mechanical Behavior of Polylactide/Poly(ε-caprolactone) Blends. Polym Eng Sci 2006;46(9):1299-1308.
32. Vilay V, Mariatti M, Ahmad Z, Pasomsouk K, Todo M. Characterization of the mechanical and thermal properties and morphological behavior of biodegradable poly(L-lactide)/poly(ε-caprolactone) and poly(L-lactide)/poly(butylene succinate-co-L-lactate) polymeric blends. J Appl Polym Sci 2009;114(3):1784-1792.

33. Wu D, Zhang Y, Yuan L. Zhang M, Zhou W. Viscoelastic interfacial properties of compatibilized poly(ε-caprolactone)/polylactide blend. J Polym Sci B Polym Phys 2010;48(7):756-765.
34. Kim C-H, Cho KY, Choi E-J, Park J-K. Effect of P(LLA-co-εCL) on the Compatibility and Crystallization Behavior of PCL/PLLA Blends. J Appl Polym Sci 1999;77(1):226-231.
35. Tsuji H, Yamada T, Suzuki M, Itsuno S. Blends of aliphatic polyesters. Part 7. Effects of poly(L-lactide-co-ε-caprolactone) on morphology, structure, crystallization, and physical properties of blends of poly(L-lactide) and poly(ε-caprolactone). Polym Int 2003;52(2):269-275.
36. Maglio G, Malinconico M, Migliozzi A, Groeninckx G. Immiscible Poly(L-lactide)/Poly(e-caprolactone) Blends: Influence of the Addition of a Poly(L-lactide)-Poly(oxyethylene) Block Copolymer on Thermal Behavior and Morphology. Macromol Chem Phys 2004;205(7)946-950.
37. Dell'Erba R, Groeninckx G, Maglio G, Malinconico M, Migliozzi A. Immiscible polymer blends of semicrystalline biocompatible components: thermal properties and phase morphology analysis of PLLA/PCL blends. Polymer 2001;42(18):7831-7840.
38. Na Y-H, He Y, Shuai X, Kikkawa Y, Doi Y, Inoue Y. Compatibilization effect of poly(ε-caprolactone)-b-

poly(ethylene glycol) block copolymers and phase morphology analysis in immiscible poly(lactide)/poly(ε-caprolactone) blends. Biomacromolecules 2002;3(6):1179-1186.

39. Vilay V, Mariatti M, Ahmad Z, Pasomsouk K, Todo M. Improvement of microstructures and properties of biodegradable PLLA and PCL blends compatibilized with a triblock copolymer. Mater Sci Eng A 2010;527(26):6930-6937.
40. Ge XG, George S, Law S, Sain M. Mechanical Properties and Morphology of Polylactide Composites with Acrylic Impact Modifier. J Macromol Sci B Phys 2011;50(11): 2070-2083.
41. Avella M, Errico ME, Laurienzo P, Martuscelli E, Raimo, Rimedio R. Preparation and characterisation of compatibilised polycaprolactone/starch composites. Polymer 2000;41(10):3875-3881.
42. Huneault MA, Li H. Morphology and properties of compatibilized polylactide/thermoplastic starch blends. Polymer 2007;48(1):270-280.
43. Juntuek P, Ruksakulpiwat C, Chumsamrong P, Ruksakulpiwat Y. Effect of glycidyl methacrylate-grafted natural rubber on physical properties of polylactic acid and natural rubber blends. J Appl Polym Sci 2012;125(1):745-754.

44. Yao M, Deng H, Mai F, Wang K, Zhang Q, Chen F, Fu Q. Modification of poly(lactic acid)/poly(propylene carbonate) blends through melt compounding with maleic anhydride. Expr Polym Lett 2011;5(11):937-949.
45. Zhang J-F, Sun X. Mechanical properties of poly(lactic acid)/starch composites compatibilized by maleic anhydride. Biomacromolecules 2004;5(4):1446-1451.
46. Carlson D, Nie L, Narayan R, Dubois P. Maleation of Polylactide (PLA) by Reactive Extrusion. J Appl Polym Sci 1999;72(4):477-485.
47. Dubois P, Krishnan M, Narayan R. Aliphatic polyester-grafted starch-like polysaccharides by ring-opening polymerization Polymer 1999;40(11):3091–3100.
48. Dubois P, Narayan R. Biodegradable Compositions by Reactive Processing of Aliphatic Polyester/Polysaccharide Blends. Macromol Symp 2003;198(1):233-243.
49. Vidéki B, Klébert Sz, Pukánszky B. Grafting of caprolacton to cellulose acetate by reactive processing. Eur Polym J 2005;41(8):1699-1707.
50. Vidéki B, Klébert Sz, Pukánszky B. External and internal plasticization of cellulose acetate with caprolactone: Structure and properties. J Polym Sci B Polym Phys 2007;45(8):873-883.

51. Hatakeyama H, Yoshida T, Hatakeyama T. The effect of side chain association on thermal and viscoelastic Properties: Cellulose acetate based polycaprolactones. J Therm Anal Calorim 2000;59(1-2):157-168.
52. Tocha E, Janik H, Dębowski M, Vancso GJ. Morphology of polyurethanes revisited by complementary AFM and TEM. J Macromol Sci – Phys 2002;41B(4-6):1291-1304.
53. Fernández CE, Bermúdez M, Alla A, Muñoz-Guerra S, Tocha E, Vancso GJ. Compared structure and morphology of nylon-12 and 10-polyurethane lamellar crystals. Polymer 2011;52(7):1515-1522.
54. Janik H, Vancso GJ. The influence of hard segment crosslinking on the morphology and mechanical properties of segmented poly(ester-urethanes) Polimery/Polymers 2005;50(2):139-142.
55. Schön PM, Bagdi K, Molnar K, Markus P, Pukanszky B, Vancso GJ. Quantitative mapping of elastic moduli at the nanoscale in phase separated polyurethanes by AFM. Eur Polym J 2011;47(4):692–698.
56. Garcia R, Herruzo ET. The emergence of multifrequency force microscopy. Nat Nanotechnol 2012;7(4):217-226.
57. Hutter JL, Bechhoefer J.Calibration of atomic force microscopoe tips. Rev Sci Instrum 1993;64(7):1868-1874.

58. Pukánszky B. Effect of interfacial interactions on the deformation and failure properties of PP/$CaCO_3$ composites. New Polym Mater 1992;3:205-217.
59. Fekete E, Pukánszky B, Peredy Z. Mutual correlations between parameters characterizing the miscibility, structure and mechanical properties of polymer blends. Angew Makromol Chem 1992;199(1):87-101.
60. Flory PJ. Principles of polymer chemistry. Ithaca: Cornell University Press; 1953.
61. Focarete ML, Scandola M, Dobrzynski P, Kovalczuk M. Miscibility and mechanical properties of blends of (l)-lactide copolymers with atactic poly(3-hydroxybutyrate). Macromolecules 2002;35(22):8472–7.
62. Zhang KY, Ran XH, Wang XM, Han CY, Han LJ, Wen X, Zhuang YG, Dong LS. Improvement in toughness and crystallization of poly(L-lactic acid) by melt blending with poly(epichlorohydrin-co-ethylene oxide). Polym Eng Sci 2011;51(12):2370–80.
63. Booij HJ. Effect of thermal stresses on the dynamic moduli of abs-resins. Br Polym J 1977;9(1):47–55.
64. Kolarik J, Lednicky F, Pukánszky B. Ternary Composites Polypropylene/Elastomer/Filler: Effect of a Block Ethylene-Propylene Elastomer. Compos Polym 1990;3:271–289.
65. Mäder D, Bruch M, Maier RD, Stricker F, Mülhaupt R. Glass Transition Temperature Depression of Elastomers

Blended with Poly(propene)s of Different Stereoregularities. Macromolecules 1999;32(4):1252–1259.

7. CAPTIONS

Fig. 1 Possible reactions of a diisocyanate with PLA end-groups; a) formation of polyurethane on the hydroxyl end-group, b) formation of amide on the carboxyl end-group, c) formation of acylurea on the carboxyl end-group.

Fig. 2 Time dependence of torque during physical (dash line) and reactive (solid line) blending (50 vol% PU).

Fig. 3 AFM phase image recorded on a PLA-b-PU reactor blend containing 50 vol% PU. Development of submicron inclusions within the PU phase. Scan size: 10 μm x 10 μm.

Fig. 4 Surface DMT elastic modulus values as obtained by Peak Force Tapping mode AFM on the physical blend containing 60 vol% PU. DMT modulus image (a) with corresponding representative cross sections (b). Corresponding phase image (c). scan size: 10 μm x 10 μm.

Fig. 5 Morphology of physical (a, c, e) and reactor (b,

d, f) blends containing 30 (a, b) 50 (c, d) and 70 vol% (e, f) polyurethane elastomer, SEM micrographs taken from surfaces fractured at liquid nitrogen temperature.

Fig. 6 The effect of composition and processing technology on the size of the dispersed particles in PLA/PU blends; (□) physical (PLA/PU), (○) reactor (PLA-b-PU) blend; error bars show the standard deviation of the values.

Fig 7 Frequency dependence of the complex viscosity of PLA/PU physical blends; effect of PU content; (○) 0, (□) 20, (△) 40, (▽) 60, (◇) 80, (●) 100 vol% PU.

Fig. 8 Composition dependence of complex viscosity measured at 1 s^{-1} frequency in PLA/PU physical and reactor blends; (□) physical (PLA/PU), (○) reactor (PLA-b-PU) blend, ------- additivity.

Fig. 9 Effect of the addition of a polyurethane elastomer on the mechanical characteristics of PLA. Comparison of physical and reactor blends. Changes in structure with composition are shown by AFM phase images with 10 μm x 10 μm scan size; (□) physical (PLA/PU), (○) reactor (PLA-b-PU) blend.

Fig. 10 DMA traces of the PLA-b-PU blend containing 60 vol% PU.

Fig. 11 The effect of composition and processing technology on the glass transition temperature of the components of PLA/PU blends; (□, ■) physical (PLA/PU), (○, ●) reactor (PLA-b-PU) blend, (□,○) PLA glass transiton, (■,●) PU soft segment transition.

Fig. 12 Quantitative estimation of interfacial interactions in physical and reactor blends through the determination of parameter *B*; (□) physical (PLA/PU), (○) reactor (PLA-b-PU) blend.

FIGURES

Fig. 1

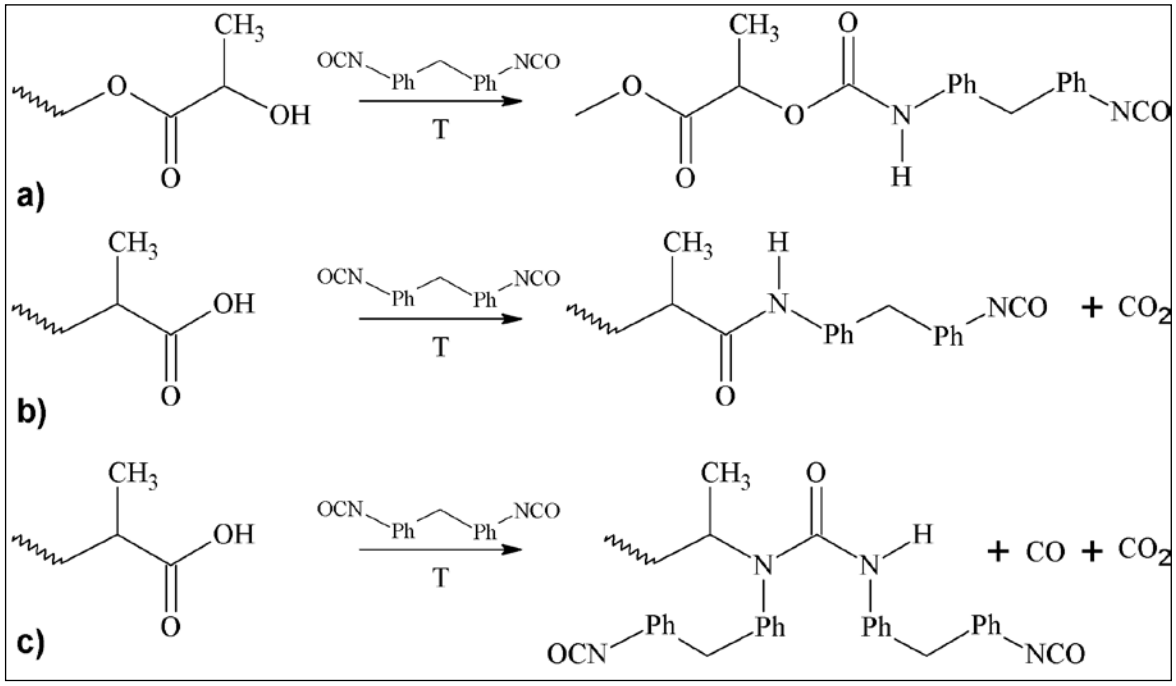

Fig. 2

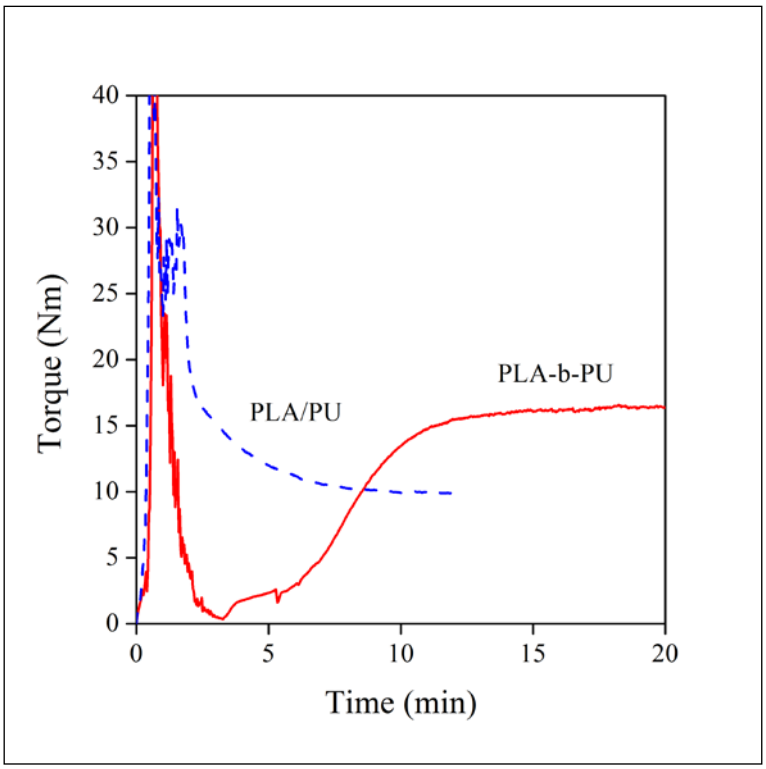

Fig. 3

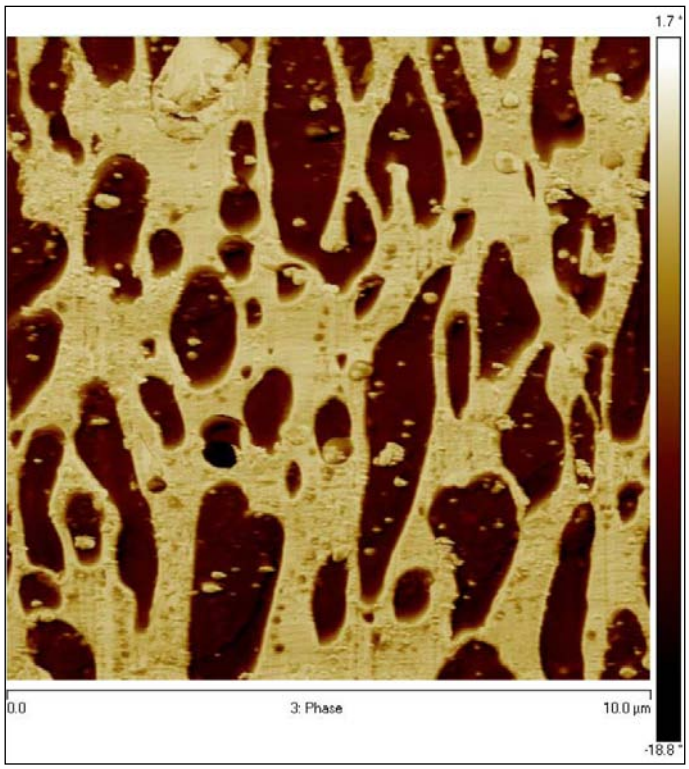

Fig. 4

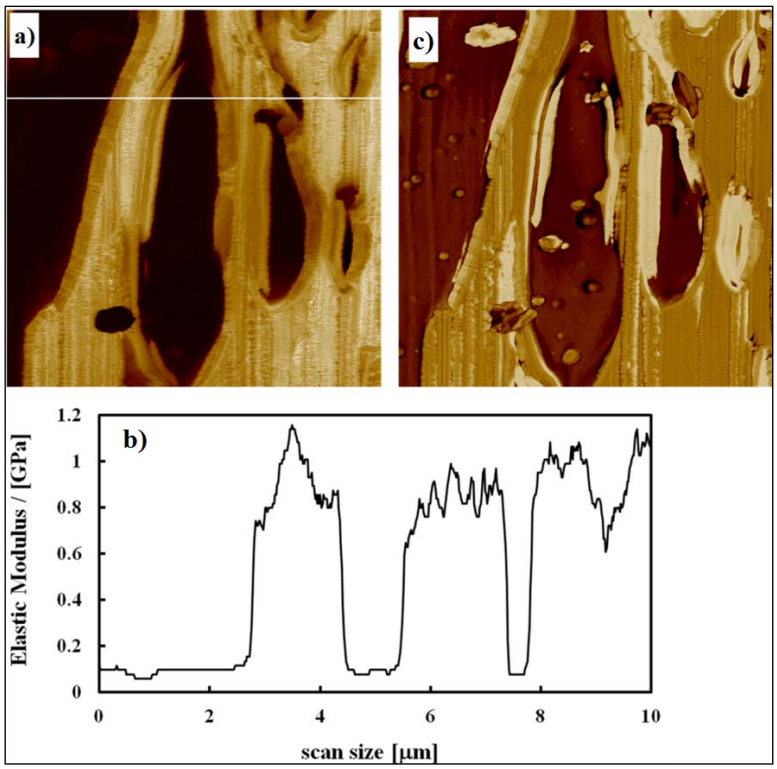

Fig.5

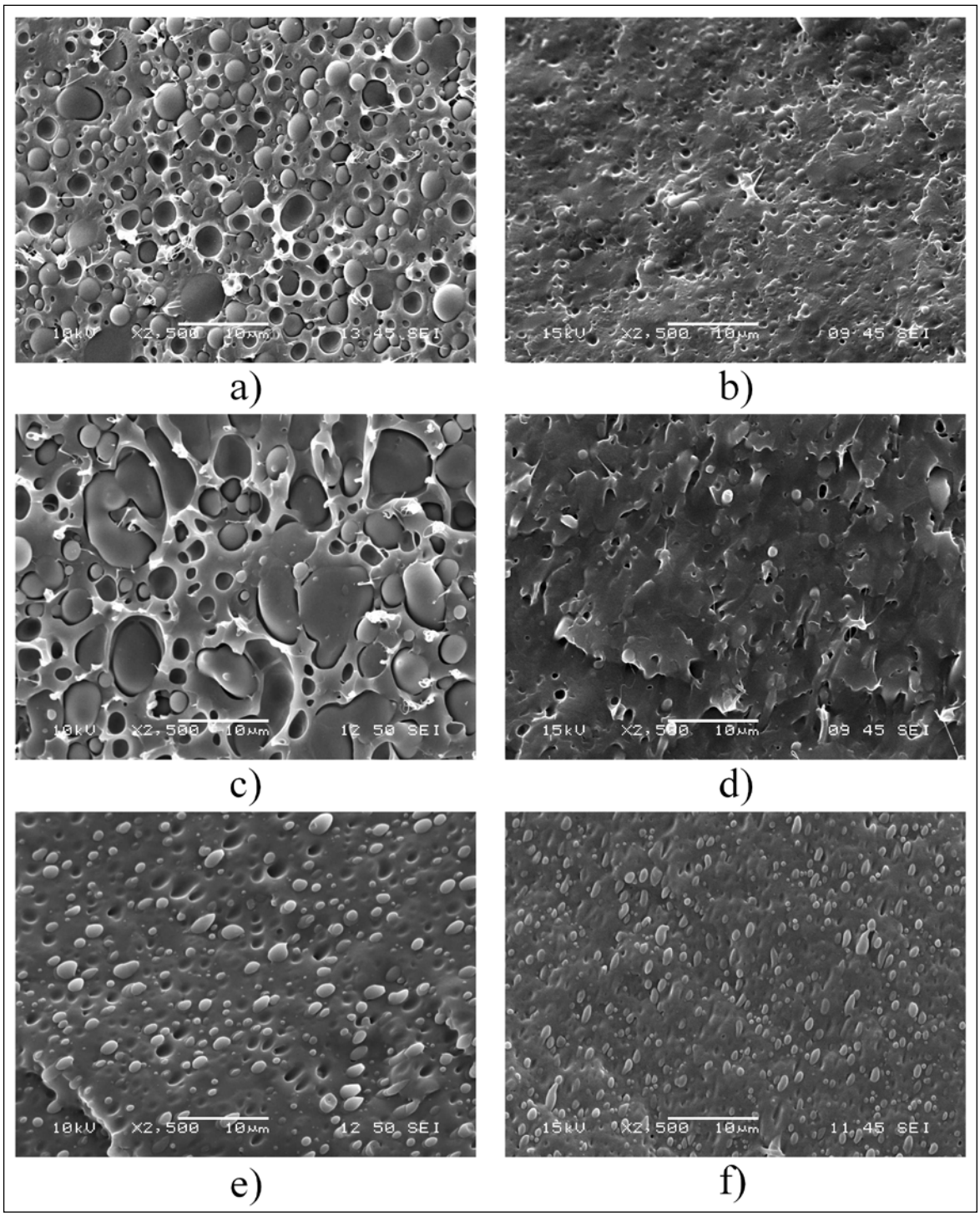
10kV X2,500 10μm 13 45 SEI
a)
15kV X2,500 10μm 09 45 SEI
b)
10kV X2,500 10μm 12 50 SEI
c)
15kV X2,500 10μm 09 45 SEI
d)
10kV X2,500 10μm 12 50 SEI
e)
15kV X2,500 10μm 11 45 SEI
f)

Fig. 6

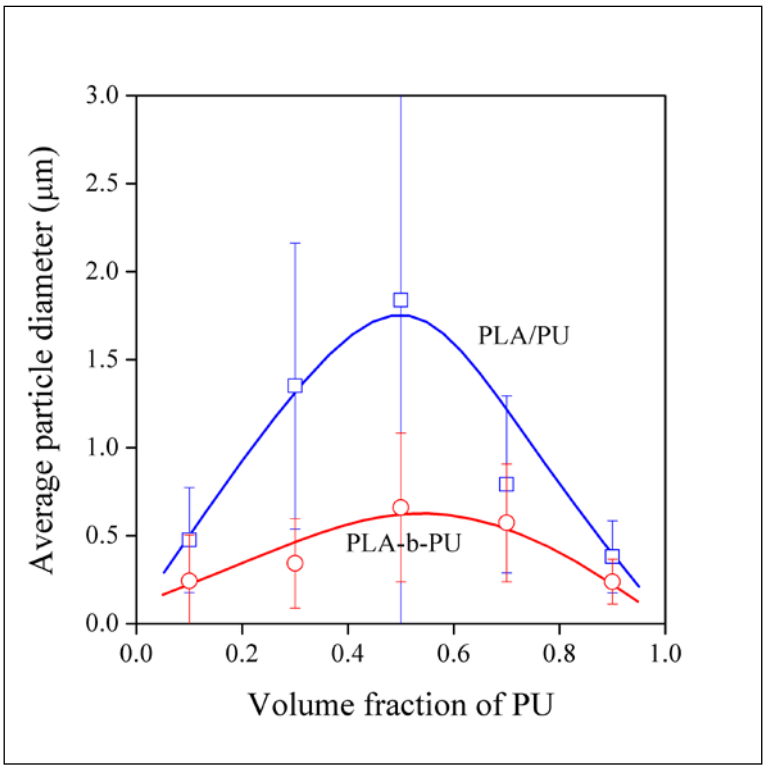
Average particle diameter (μm)
3.0
2.5
2.0
1.5
1.0
0.5
0.0
0.0
0.2
0.4
0.6
0.8
1.0
Volume fraction of PU
PLA/PU
PLA-b-PU

Fig. 7

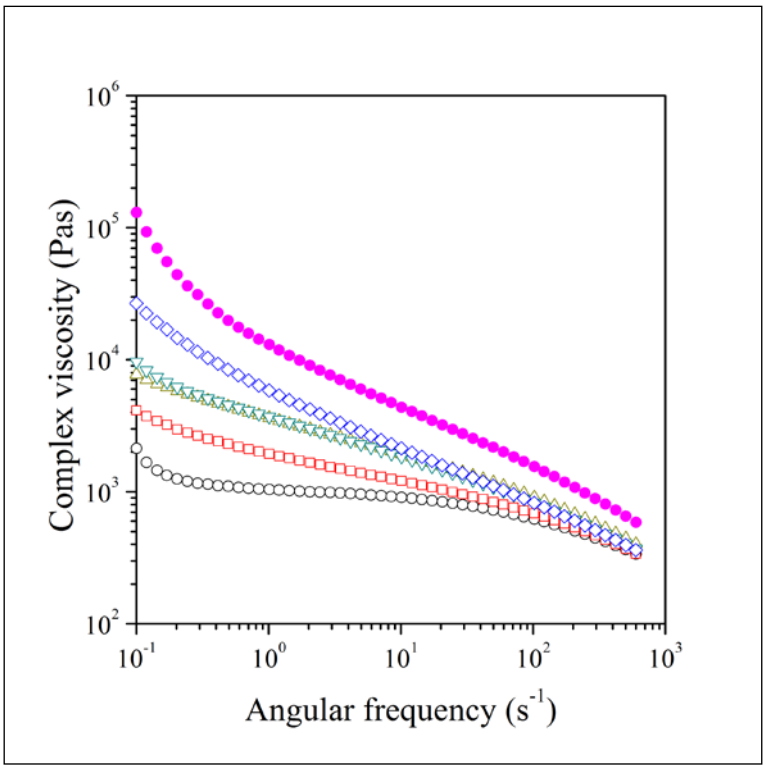
Complex viscosity (Pas)
10^6
10^5
10^4
10^3
10^2
10^{-1}
10^0
10^1
10^2
10^3
Angular frequency (s^{-1})

Fig. 8

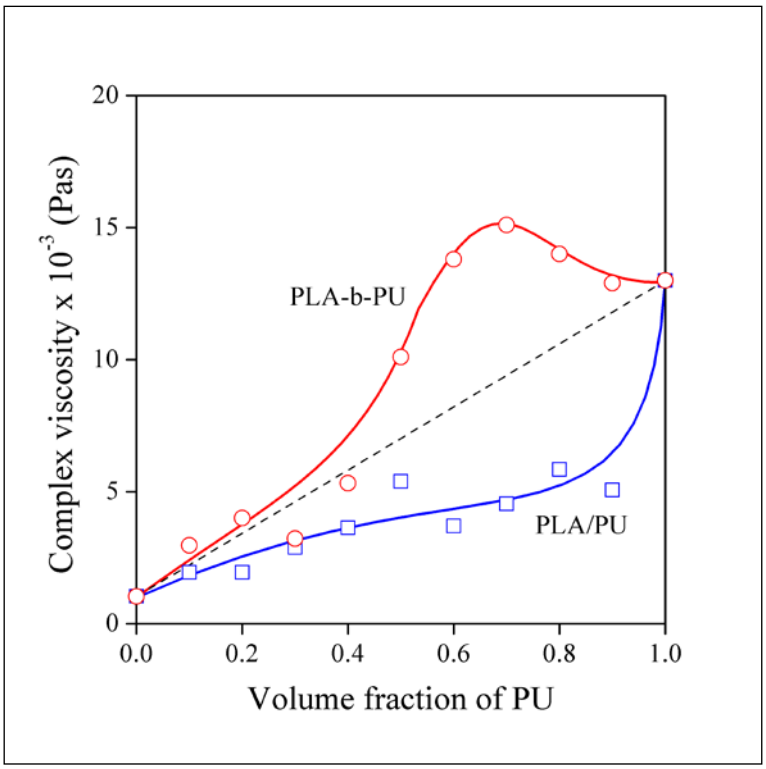
Complex viscosity x 10^{-3} (Pas)
20
15
10
5
0
0.0
0.2
0.4
0.6
0.8
1.0
Volume fraction of PU
PLA-b-PU
PLA/PU

Fig. 9

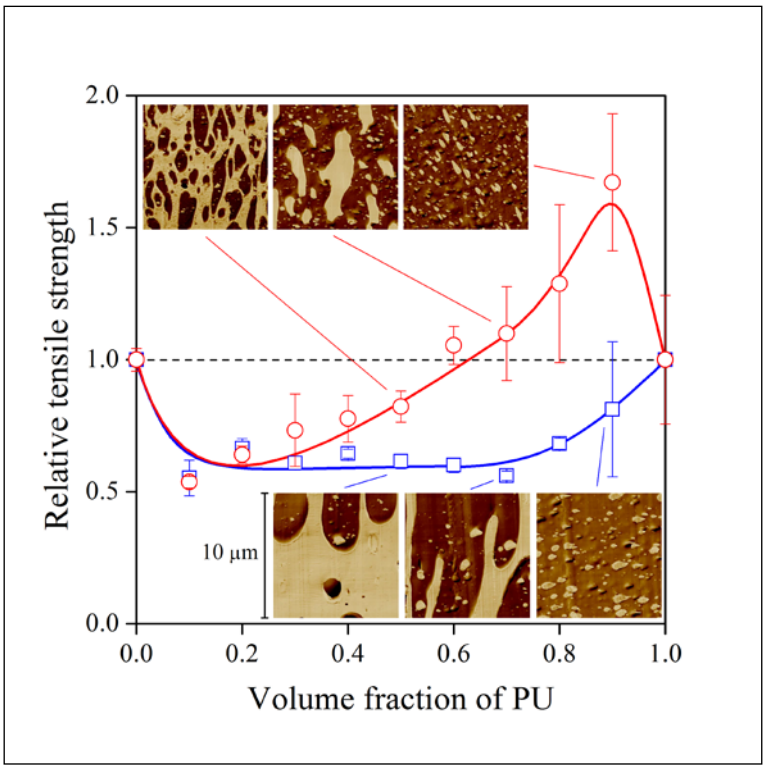
Relative tensile strength
Volume fraction of PU
10 μm
2.0
1.5
1.0
0.5
0.0
0.0
0.2
0.4
0.6
0.8
1.0

Fig. 10

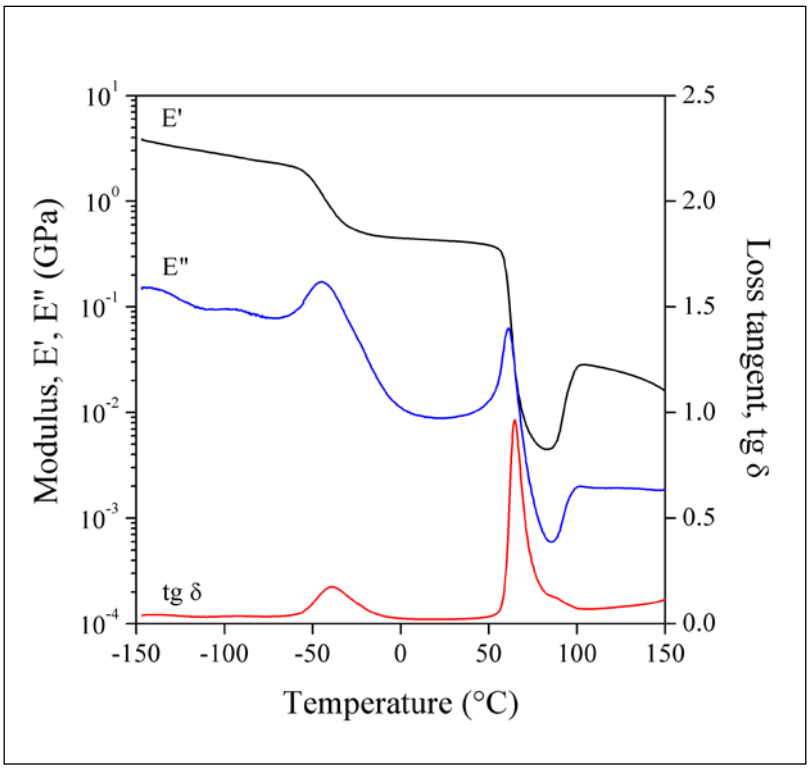
E'
E"
tg δ
Modulus, E', E" (GPa)
Loss tangent, tg δ
Temperature (°C)
10^1
10^0
10^-1
10^-2
10^-3
10^-4
2.5
2.0
1.5
1.0
0.5
0.0
-150
-100
-50
0
50
100
150

Fig. 11

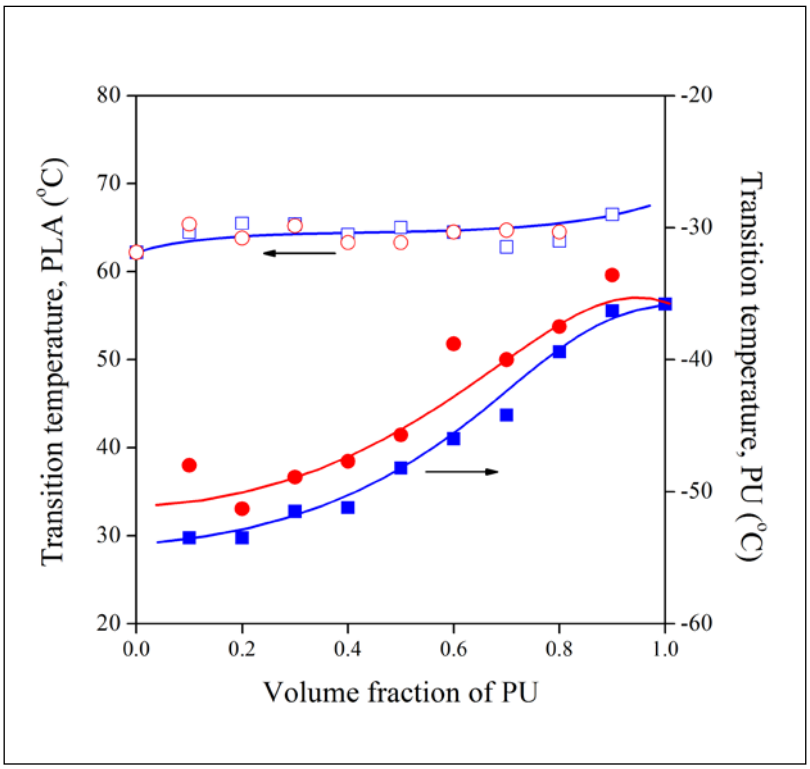
Transition temperature, PLA (°C)
Transition temperature, PU (°C)
Volume fraction of PU
80
70
60
50
40
30
20
-20
-30
-40
-50
-60
0.0
0.2
0.4
0.6
0.8
1.0

Fig. 12

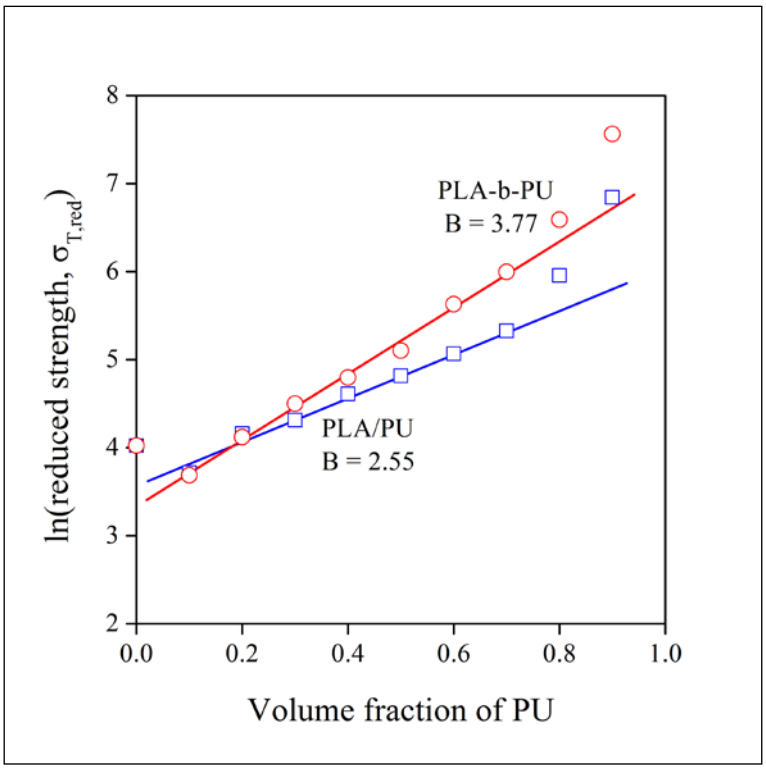
ln(reduced strength, $\sigma_{T,red}$)
Volume fraction of PU
PLA-b-PU
B = 3.77
PLA/PU
B = 2.55
8
7
6
5
4
3
2
0.0
0.2
0.4
0.6
0.8
1.0